Magnetically responsive multidimensional thermal display using liquid-metal-based flexible thermal switches

Cite as: APL Mater. 14, 031110 (2026); doi: 10.1063/5.0319412
Submitted: 23 December 2025 • Accepted: 27 February 2026 •
Published Online: 11 March 2026

Yuxia Dong,[1] Xudong Zhang,[2,3] and Bingyang Cao[1,a)]

AFFILIATIONS

[1] Key Laboratory for Thermal Science and Power Engineering of Ministry of Education, Department of Engineering Mechanics, Tsinghua University, Beijing 100084, China
[2] State Key Laboratory of Cryogenic Science and Technology, Technical Institute of Physics and Chemistry, Chinese Academy of Sciences, Beijing 100190, China
[3] School of Future Technology, University of Chinese Academy of Sciences, Beijing 100049, China

[a)] **Author to whom correspondence should be addressed:** caoby@tsinghua.edu.cn

ABSTRACT

Traditional thermal switches regulate thermal conductivity only in a single global direction, which limits their application in infrared thermal display. This study presents a flexible thermal switch composed of magnetic liquid metal, polydimethylsiloxane, graphene films, and polyvinyl chloride films. The magnetic field can regulate the distribution of magnetic liquid metal, thereby adjusting the thermal conductivity of the flexible thermal switch. The thermal conductivity can be switched between 0.245 and 1.546 $W \cdot m^{-1} \cdot K^{-1}$, corresponding to a thermal switching ratio of 6.3. The flexible thermal switch can be applied to a multidimensional thermal display, which enables independent regional regulation by a magnetic field. Regions exposed to a magnetic field exhibit high thermal conductivity, whereas regions without a magnetic field maintain low thermal conductivity. Finite element simulation demonstrates that alphabetic thermal patterns from A to Z can be achieved through regional modulation of thermal conductivity. Experimentally, a "THU" thermal pattern is generated by moving a magnetic pen and visualized using infrared thermal imaging. This work overcomes the limitation of conventional thermal switches that permit only global regulation in a single direction, offering new opportunities for smart thermal management, information display, and infrared camouflage.

I. INTRODUCTION

Precise heat manipulation is essential for reducing energy consumption in buildings[1,2] and ensuring effective thermal management in electronic devices,[3–5] power batteries,[6,7] and spacecraft.[8] In addition, regional regulation of heat flow enables the generation of invisible thermal patterns that can only be visualized using an infrared (IR) thermal imager.[9] This phenomenon, known as infrared thermal display, has recently attracted extensive attention for its potential in information encryption,[10–12] messaging,[13] and thermal camouflage.[14,15] Infrared thermal display can be realized by modulating thermal conduction or infrared radiation properties, thereby creating programmable thermal images imperceptible to the naked eye. Three main strategies have been developed to achieve infrared thermal display: infrared reflectivity modulation,[16,17] latent heat release,[18] and precise heat manipulation.[19,20] Among these, precise heat manipulation is not limited by temperature, allows the creation of complex patterns, and offers convenient operation, making it particularly promising for practical applications.

Thermal switches, as key components for heat manipulation, can reversibly toggle their thermal conductivity between the "on" and "off" states.[21–24] Achieving infrared thermal display requires thermal switches that respond rapidly to external stimuli and can locally adjust their thermal conductivity. However, traditional thermal switches can only achieve overall regulation of thermal conductivity in a single direction,[24–28] and it is difficult to achieve independent regulation of spatial partitions. Zhao *et al.*[29] fabricated a thermal switch based on liquid metal and shape memory

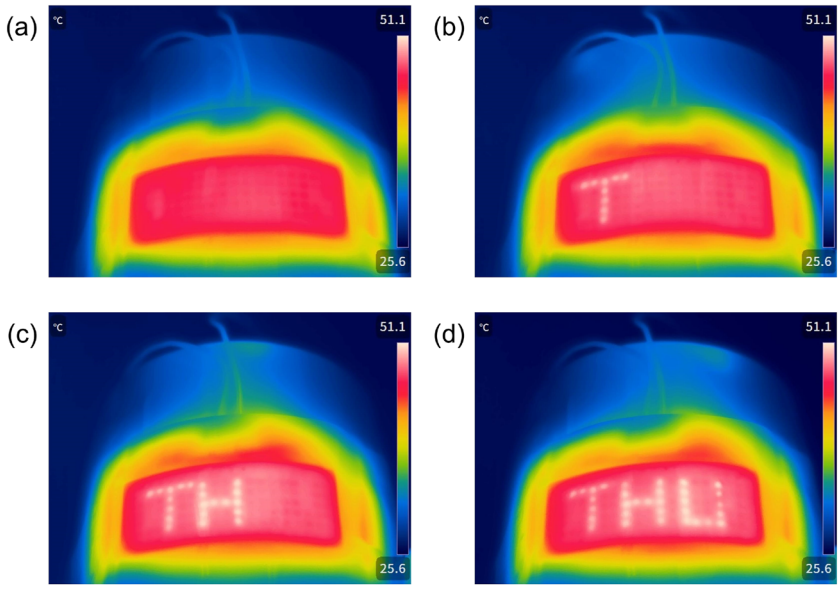

FIG. 1. Multidimensional thermal display. (a) Original temperature distribution. (b) Pattern "T." (c) Pattern "TH." (d) Pattern "THU."

foam, which exhibited higher thermal conductivity under compression and was applied to infrared signal camouflage. Although this work inspires interest in infrared thermal display based on thermal switches, the mechanical compression mechanism poses risks of liquid metal leakage and inconvenient displacement. In contrast, employing non-contact control methods to achieve infrared thermal display by regional regulation of thermal switches offers significant advantages.[30,31] Magnetic liquid metal combines magnetism, high thermal conductivity, and fluidity, making it suitable for the design of flexible thermal switches with magnetic responsiveness.[32–34]

In this work, we propose a flexible and magnetically responsive thermal switch composed of magnetic liquid metal, polydimethylsiloxane (PDMS), graphene films, and polyvinyl chloride (PVC) films. By controlling the spatial distribution of magnetic liquid metal under an external magnetic field, the magnetic liquid metal can selectively contact or detach from the upper PVC film, thereby switching local thermal conductivity between 0.245 and 1.546 $W \cdot m^{-1} \cdot K^{-1}$. This magnetically responsive and spatially addressable regulation breaks through the limitation of traditional thermal switches that only enable global thermal regulation, achieving precise heat manipulation and programmable multidimensional thermal display. Finite element simulation verifies that the regionally controlled thermal switch can realize thermal display of A–Z alphabetic patterns. Furthermore, a "THU" thermal pattern is experimentally drawn by moving a magnetic pen, as shown in Fig. 1. This work offers a new paradigm for smart thermal management, information display, and thermal camouflage.

II. RESULTS AND DISCUSSION

A. Preparation of magnetic liquid metal

The magnetic liquid metal used in this study is composed of iron particles with a particle size of 38 μm and eutectic gallium indium (EGaIn), which contains 75.5 wt. % Ga and 24.5 wt. % In. The preparation procedure of magnetic liquid metal is illustrated in Fig. 2. First, 40 g of EGaIn and 10 g of iron particles were weighed

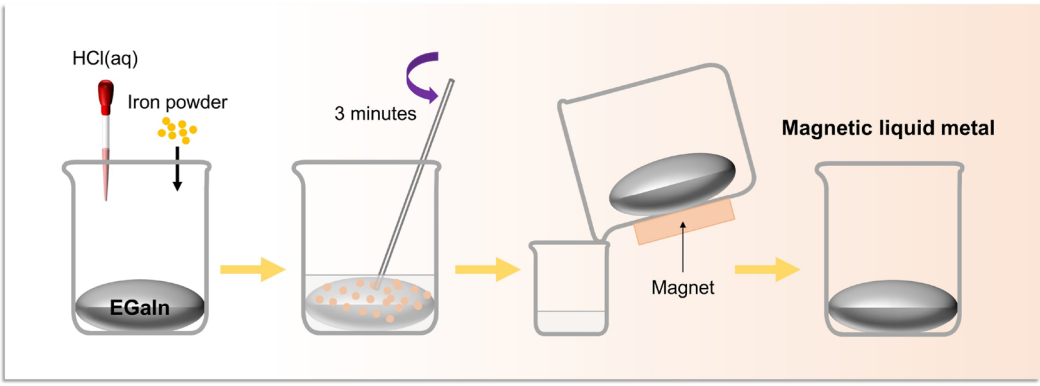

FIG. 2. The preparation process of magnetic liquid metal.

and placed in a beaker. Subsequently, 5 ml of hydrochloric acid (20.0 wt. % HCl) was added. The hydrochloric acid removed the oxide layers from the surfaces of both iron particles and EGaIn, enabling direct contact between them. The mixture was stirred at room temperature for ~3 min, during which the solution changed from turbid to transparent, indicating the successful incorporation of iron particles into EGaIn. The magnetic liquid metal was separated from the remaining hydrochloric acid solution using a permanent magnet, and the remaining hydrochloric acid solution was poured away. Finally, the magnetic liquid metal with an iron powder mass fraction of 20% was obtained. During the preparation process, the galvanic cell reaction between Ga and Fe prevented the iron particles from being corroded by hydrochloric acid, thereby preserving their magnetic properties.[35,36] The hysteresis loops of liquid metal were analyzed using a vibrating sample magnetometer, as shown in Fig. S1. The thermal conductivities of EGaIn and magnetic liquid metal were measured using the transient plane source method, yielding values of 21.8 and 25.8 $W \cdot m^{-1} \cdot K^{-1}$, respectively. The incorporation of iron particles enhances the magnetism and thermal conductivity of liquid metal.

B. Thermal performance of the flexible thermal switch

As shown in Fig. 3(a), magnetic liquid metal was placed in a transparent container, with an acrylic sheet positioned above it. The morphological evolution of the magnetic liquid metal was recorded using a high-speed camera. As shown in Fig. 3(b), when a permanent magnet was positioned above the acrylic sheet, the magnetic liquid metal bulged upward. When the magnet was removed, the magnetic liquid metal returned to its original shape under the influence of gravity. Based on this characteristic, a flexible thermal switch is fabricated using magnetic liquid metal, PDMS, graphene films, and PVC films, as illustrated in Fig. 3(c). The bottom encapsulation layer is composed of graphene film with high thermal conductivity, which facilitates heat transfer to the magnetic liquid metal. Because graphene film possesses high in-plane thermal diffusivity and in-plane thermal conductivity, heat rapidly spreads along the plane, making it unsuitable as the top encapsulation layer for thermal display. Therefore, a PVC film with lower thermal conductivity is selected as the top encapsulation material. In the absence of a magnetic field, magnetic liquid metal does not contact the upper PVC film, and the flexible thermal switch remains in the "off" state, exhibiting low thermal conductivity. Under a magnetic field, the magnetic liquid metal contacts the upper PVC film, forming a heat conduction pathway. The flexible thermal switch is thus in the "on" state, exhibiting high thermal conductivity. The thermal conductivity is modulated by controlling the connection and disconnection of the heat conduction pathway, which is achieved by magnetically manipulating the morphology of the magnetic liquid metal. The thermal conductivity of the flexible thermal switch was measured using the steady state method. Because PDMS exhibits

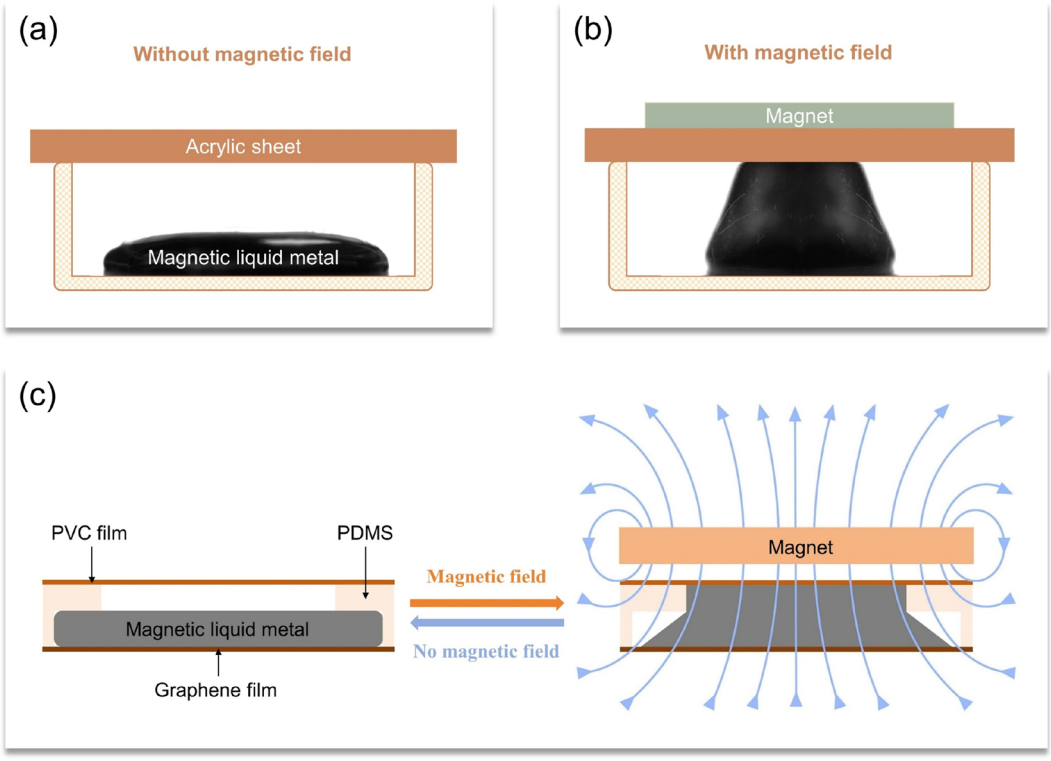

FIG. 3. Flexible thermal switch. The morphology of magnetic liquid metal (a) without and (b) with a magnetic field. (c) Schematic of the flexible thermal switch in the "off" and "on" states.

poor mechanical strength and the steady state method requires applied pressure, a resin material with similar thermal conductivity is substituted for PDMS during the test. The thermal conductivity measurement results are shown in Table S1. The thermal conductivity is 1.546 $W \cdot m^{-1} \cdot K^{-1}$ in the "on" state (k_{on}) and 0.245 $W \cdot m^{-1} \cdot K^{-1}$ in the "off" state (k_{off}), corresponding to a thermal switching ratio of $r = k_{on}/k_{off} = 6.3$.

The finite element simulation was employed to calculate the thermal conductivity of the flexible thermal switch. Structural models of the flexible thermal switch in both the "off" and "on" states were constructed based on the same geometric parameters as those used in the experiment. However, unlike the experimental measurement, in which the "on" state required a specially designed structure to test thermal conductivity in the absence of a magnetic field, the simulated "on" state involved no such structural modification. The upper surface of the flexible thermal switch was set at 20 °C, and the heat flux density at the lower surface was 5000 $W \cdot m^{-2}$. Further simulation details are provided in the supplementary material. The calculated thermal conductivities are 0.242 $W \cdot m^{-1} \cdot K^{-1}$ in the "off" state and 1.581 $W \cdot m^{-1} \cdot K^{-1}$ in the "on" state, which are in good agreement with the experimental results. Furthermore, the finite element method was employed to simulate the temperature distribution of the flexible thermal switch in the "off" and "on" states. The lower surface temperature of the flexible thermal switch was fixed at 55 °C, while the upper surface was subjected to convective heat transfer with ambient air at 25 °C, with a convective heat transfer coefficient of 25 $W \cdot m^{-2} \cdot K^{-1}$. Figure 4(a) presents the temperature distribution along the longitudinal cross section of the flexible thermal switch. In the "on" state, the temperature distribution of the flexible thermal switch is more uniform, with a higher upper surface temperature, indicating enhanced thermal conductivity.

C. Thermal display

The realization of infrared thermal display depends on the ability to independently regulate the "on" and "off" states of flexible thermal switches in different regions. Therefore, flexible thermal switches were integrated into a thermal display material, with the PDMS skeleton designed as a 5 × 5 grid structure, where each cell has a side length of 2 mm. In the simulation, the temperature of the lower surface of the thermal display material was set at 55 °C, and the upper surface was subjected to convective heat transfer with ambient air at 25 °C, with a convective heat transfer coefficient of 25 $W \cdot m^{-2} \cdot K^{-1}$. Regions in the "on" state possess higher ther-

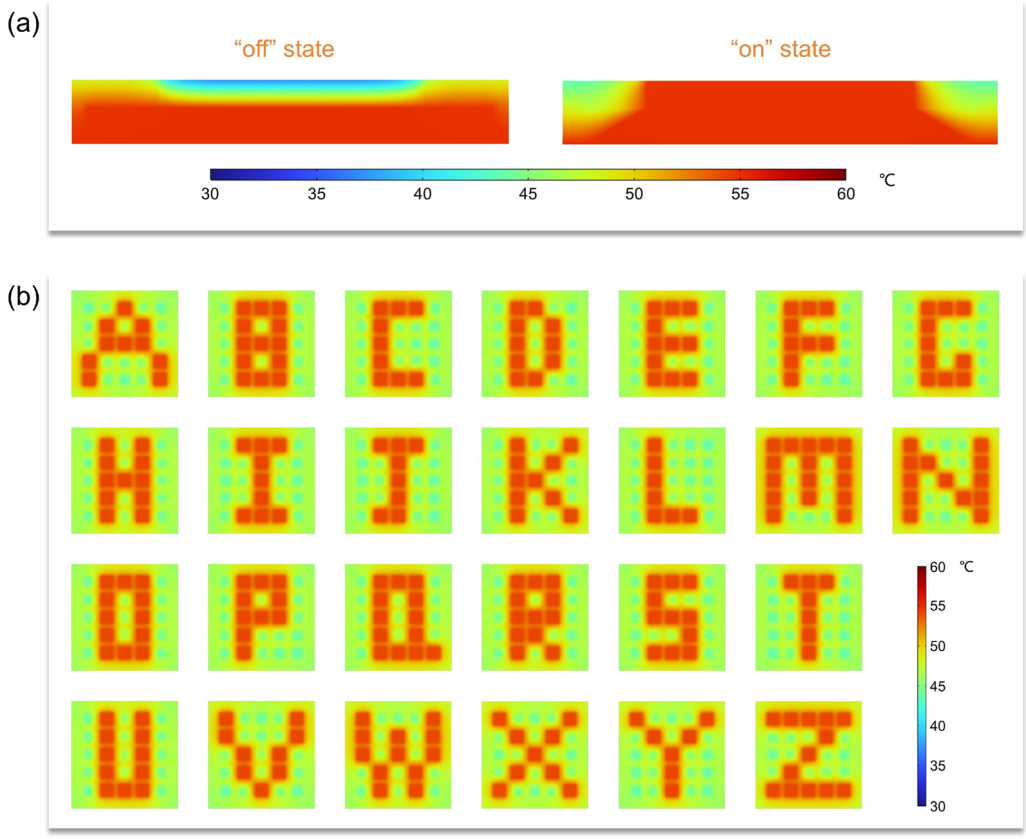

FIG. 4. Finite element simulation. (a) Temperature distribution of the flexible thermal switch in the "off" and "on" states. (b) Thermal patterns of the complete alphabet from A to Z.

mal conductivity, resulting in higher upper surface temperature. By selectively controlling the locations of the "on" states, various thermal patterns are formed on the upper surface of the thermal display material. As shown in Fig. 4(b), by spatially modulating the thermal conductivity of individual thermal switches, thermal patterns corresponding to the letters from A to Z are successfully generated.

To experimentally validate the application of the flexible thermal switch in infrared thermal display, a flexible thermal display material was fabricated, as illustrated in Fig. 5(a). The PDMS skeleton consists of multiple grids and a rectangular cavity, which together form its internal framework. The rectangular cavity is filled with magnetic liquid metal, while the grid regions are filled with air. The bottom surface is encapsulated with a graphene film, and the top of the PDMS skeleton is sealed with a PVC film. As shown in Fig. 5(b), the thermal display material exhibits excellent flexibility, allowing it to conform to multidimensional curved surfaces. These features make thermal display material suitable for use in multidimensional thermal display.

A polyimide heating film was attached to the surface of a cylinder, and the flexible thermal display material was placed on top. As shown in Figs. 5(c) and S3, a magnetic pen containing a permanent magnet was used to draw patterns on the thermal display material. In regions where a magnetic field is present, the magnetic liquid metal contacts the upper PVC film. Regions exposed to the magnetic field exhibit higher thermal conductivity, whereas those without a magnetic field maintain lower thermal conductivity. By adjusting the position of the magnetic pen, various patterns can be created on the thermal display material. When the magnetic pen is moved across the flexible thermal display material, the thermal conductivity along its trajectory increases, leading to a higher surface temperature in the corresponding regions. Although invisible to the naked eye, these patterns are observable using an infrared thermal imager. As shown in Video S1, the letters "T," "H," and "U" are sequentially displayed on the flexible thermal display material.

III. CONCLUSION

In conclusion, a flexible thermal switch composed of magnetic liquid metal, PDMS, graphene films, and PVC films has been developed. The magnetic field regulates the distribution of magnetic liquid metal, thereby enabling the flexible thermal switch to toggle between 0.245 and 1.546 $W \cdot m^{-1} \cdot K^{-1}$ in thermal conductivity, corresponding to a thermal switching ratio of 6.3. Building upon this design, we further fabricate a flexible thermal display material in which the thermal conductivity of each region can be independently tuned, thereby realizing multidimensional thermal display. Regions exposed to a magnetic field exhibit high thermal conductivity, while those without a magnetic field maintain low thermal conductivity, forming distinct thermal patterns. Finite element simulation demonstrates that the regionally controlled thermal switch can generate alphabetic thermal patterns (A–Z). Experimentally, a dynamic "THU" thermal pattern is formed on the curved surface by maneuvering a magnetic pen and visualized using an infrared thermal imager. This work presents a novel strategy for multidimensional thermal display, offering new opportunities for information visualization and infrared camouflage.

IV. EXPERIMENTAL SECTION

A. Fabrication of the PDMS skeleton

The PDMS skeleton was fabricated using Sylgard 184 silicone elastomer, which consists of a pre-polymer base and a crosslinking curing agent. The fabrication process began by mixing the base and curing agent at a mass ratio of 10:1, followed by mechanical stirring for 10 min. The resulting mixture was then degassed in a vacuum oven for 20 min to remove bubbles. Following degassing, the mixture was cast into a custom mold and cured at 100 °C for 2 h in a vacuum oven. Finally, the cured PDMS was demolded to obtain the desired PDMS skeleton.

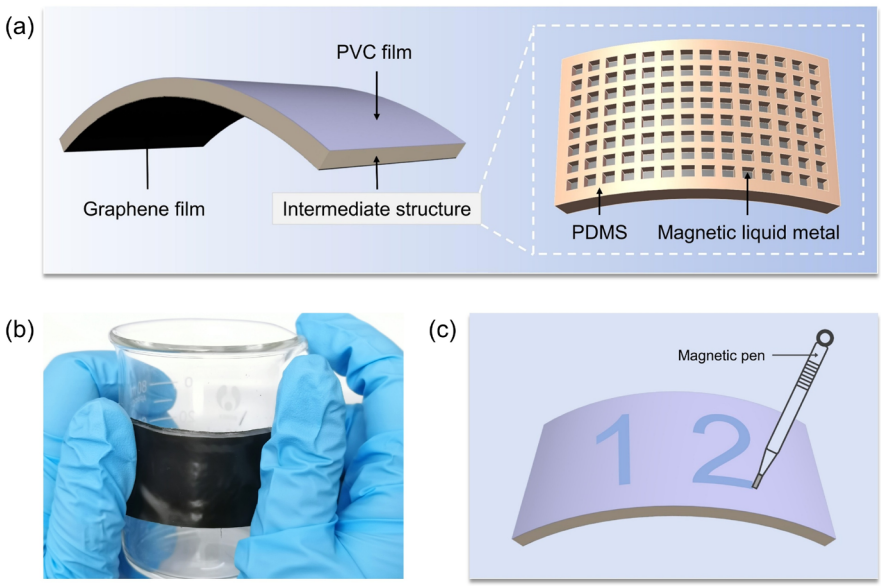

FIG. 5. Flexible thermal display material. (a) Structure of the flexible thermal display material. (b) Flexibility of the flexible thermal display material. (c) Drawing patterns on the surface of flexible thermal display material with a magnetic pen.

B. Fabrication of the flexible thermal switch

The flexible thermal switch consists of a graphene film, a PDMS skeleton, magnetic liquid metal, and a PVC film, with overall dimensions of 25.5 × 25.5 × 3.73 mm^3. The graphene film serves as the bottom encapsulation layer, while the PVC film functions as the top encapsulation layer. The thicknesses of the graphene film, PDMS skeleton, and PVC film are 0.1, 3.5, and 0.13 mm, respectively. The internal cavity of the PDMS skeleton features two interconnected rectangular regions, measuring 15.6 × 15.6 × 1.5 and 23.4 × 23.4 × 2.0 mm^3, respectively. The cavity within the PDMS skeleton is filled with magnetic liquid metal and air. The morphology of the magnetic liquid metal can be dynamically controlled by an external magnetic field, achieving switching between the "on" and "off" states.

C. Fabrication of the flexible thermal display material

The flexible thermal display material is fabricated by integrating multiple flexible thermal switches. Its material composition and thickness are identical to those of a single flexible thermal switch, while its length and width vary. The PDMS skeleton measures 60.0 × 24.0 × 3.5 mm^3, with each grid having a side length of 2.0 mm and a thickness of 1.5 mm, along with the rectangular cavity measuring 56.0 × 20.0 × 2.0 mm^3.

D. Characterization

The hysteresis loops of liquid metal were analyzed using a vibrating sample magnetometer (LakeShore 7404). The thermal conductivities of liquid metal were measured using the transient plane source method (Hot Disk TPS 2500 S). The morphological evolution of the magnetic liquid metal was recorded using a high-speed camera (FASTCAM Mini UX 50). The thermal conductivity of the flexible thermal switch was measured using a Thermal Interface Material Thermal Resistance and Conductivity Measurement Apparatus (Longwin LW-9389MD). The thermal patterns were recorded using an infrared thermal imager (Fotric 288+).

SUPPLEMENTARY MATERIAL

See the supplementary material for detailed information on the hysteresis loop, thermal conductivity measurement, finite element simulation, and magnetic pen. Video S1 presents infrared thermal imaging of the dynamic drawing process of the "THU" thermal pattern.

ACKNOWLEDGMENTS

This work was supported by the National Natural Science Foundation of China (Grant Nos. 52425601, 52327809, 52206098, and 82361138571), the National Key Research and Development Program of China (Grant No. 2023YFB4404104), and the Beijing Natural Science Foundation (Grant No. L233022).

AUTHOR DECLARATIONS

Conflict of Interest

The authors have no conflicts to disclose.

Author Contributions

Yuxia Dong: Conceptualization (lead); Data curation (equal); Formal analysis (lead); Investigation (lead); Methodology (lead); Software (lead); Validation (lead); Visualization (lead); Writing – original draft (lead). **Xudong Zhang**: Conceptualization (equal); Data curation (equal); Formal analysis (equal); Investigation (supporting); Methodology (equal); Software (supporting); Supervision (equal); Validation (supporting); Writing – original draft (supporting); Writing – review & editing (equal). **Bingyang Cao**: Conceptualization (equal); Data curation (equal); Funding acquisition (lead); Project administration (lead); Software (supporting); Supervision (equal); Visualization (supporting); Writing – review & editing (lead).

DATA AVAILABILITY

The data that support the findings of this study are available within the article and its supplementary material.

REFERENCES

[1] A. Henry, R. Prasher, and A. Majumdar, "Five thermal energy grand challenges for decarbonization," Nat. Energy **5**, 635 (2020).
[2] S. J. M. Koenders, R. C. G. M. Loonen, and J. L. M. Hensen, "Investigating the potential of a closed-loop dynamic insulation system for opaque building elements," Energy Build. **173**, 409 (2018).
[3] A. R. Dhumal, A. P. Kulkarni, and N. H. Ambhore, "A comprehensive review on thermal management of electronic devices," J. Eng. Appl. Sci. **70**, 140 (2023).
[4] J. Li, Y. Zhou, C. Jiang, D. Lei, and X. Yu, "Recent advances in passive cooling materials for thermal management in flexible electronics," J. Mater. Chem. C **12**, 12179 (2024).
[5] B. Cao, "Thermal design automation (TDA) for multiscale thermal management of electronics," J. Appl. Phys. **138**, 180901 (2025).
[6] R. Kumar and P. K. Panigrahi, "A hybrid battery thermal management system using ionic wind and phase change material," Appl. Energy **359**, 122676 (2024).
[7] Q. L. Yue, C. X. He, M. C. Wu, and T. S. Zhao, "Advances in thermal management systems for next-generation power batteries," Int. J. Heat Mass Transfer **181**, 121853 (2021).
[8] D. W. Hengeveld, M. M. Mathison, J. E. Braun, E. A. Groll, and A. D. Williams, "Review of modern spacecraft thermal control technologies," HVACR Res. **16**, 189 (2010).
[9] F. Hou, Y. Zhang, Y. Zhou, M. Zhang, B. Lv, and J. Wu, "Review on infrared imaging technology," Sustainability **14**, 11161 (2022).
[10] Z. Li, L. Wang, X. Liu, J. Li, H. S. Yun, Z. Wang, X. Zhang, T.-S. Wong, and S. Shen, "Brochosome-inspired binary metastructures for pixel-by-pixel thermal signature control," Sci. Adv. **10**, eadl4027 (2024).
[11] J. Wang, M. Wang, Q. Xie, W. Li, L. Zhang, L. Zhang, J. Xie, D. Liu, and P. Zhou, "Multilevel information encryption mediated by reconfigurable thermal emission in smart bilayer material," Laser Photonics Rev. **18**, 2301106 (2024).
[12] H. Q. Wang, Y. Tang, Z. Y. Huang, F. Z. Wang, P. F. Qiu, X. Zhang, C. H. Li, and Q. Li, "A dual-responsive liquid crystal elastomer for multi-level encryption and transient information display," Angew. Chem., Int. Chem. **135**, e202313728 (2023).
[13] Y. Zhong, X. Liu, Z. Wang, T. Huang, J. Zou, S. Lin, X. Luo, Z. Li, R. Cheng, X. Zhang, and S. Shen, "Reconfigurable integrated high-speed thermal metamaterial pixel arrays," Nano Lett. **25**, 12712 (2025).
[14] R. Hu, S. Zhou, Y. Li, D. Y. Lei, X. Luo, and C. W. Qiu, "Illusion thermotics," Adv. Mater. **30**, 1707237 (2018).
[15] O. Salihoglu, H. B. Uzlu, O. Yakar, S. Aas, O. Balci, N. Kakenov, S. Balci, S. Olcum, S. Süzer, and C. Kocabas, "Graphene-based adaptive thermal camouflage," Nano Lett. **18**, 4541 (2018).

[16]Y. Zhang, H. Zhu, S. An, W. Xing, B. Fu, P. Tao, W. Shang, J. Wu, M. D. Dickey, C. Song, and T. Deng, "Chameleon-inspired tunable multi-layered infrared-modulating system via stretchable liquid metal microdroplets in elastomer film," Nat. Commun. **15**, 5395 (2024).
[17]B. Yao, S. He, R. Wang, Y. Zeng, W. Shi, Y. Zhu, X. Xu, S. Wang, Q. Wang, and H. Wang, "Cephalopod-inspired soft composite with liquid metal inclusions for tunable infrared modulation," J. Materiom. **11**, 101012 (2025).
[18]H. Wang, B. Yuan, X. Zhu, X. Shan, S. Chen, W. Ding, Y. Cao, K. Dong, X. Zhang, R. Guo *et al.*, "Multi-stimulus perception and visualization by an intelligent liquid metal-elastomer architecture," Sci. Adv. **10**, eadp5215 (2024).
[19]R. Hu, S. Huang, M. Wang, X. Luo, J. Shiomi, and C. W. Qiu, "Encrypted thermal printing with regionalization transformation," Adv. Mater. **31**, 1807849 (2019).
[20]R. Qiu, "Tunable thermal pattern for thermal illusion and encrypted messaging," J. Phys.: Conf. Ser. **2174**, 012089 (2022).
[21]G. Wehmeyer, T. Yabuki, C. Monachon, J. Wu, and C. Dames, "Thermal diodes, regulators, and switches: Physical mechanisms and potential applications," Appl. Phys. Rev. **4**, 041304 (2017).
[22]Z. Zhang and B. Cao, "Thermal smart materials with tunable thermal conductivity: Mechanisms, materials, and applications," Sci. China Phys., Mech. Astron. **65**, 117003 (2022).
[23]J. Jia, S. Li, X. Chen, and Y. Shigesato, "Emerging solid–state thermal switching materials," Adv. Funct. Mater. **34**, 2406667 (2024).
[24]Z.-T. Zhang, Y.-X. Dong, and B.-Y. Cao, "Promoting temperature control and energy conservation by smart thermal management using nanoparticle suspensions with tunable thermal conductivity," Appl. Energy **374**, 124097 (2024).
[25]J. Philip, P. D. Shima, and B. Raj, "Nanofluid with tunable thermal properties," Appl. Phys. Lett. **92**, 043108 (2008).
[26]Q. Zheng, S. E. Murray, Z. Diao, A. Bhutani, D. P. Shoemaker, and D. G. Cahill, "Thermal transport through the magnetic martensitic transition in Mn_xMGe (M = Co, Ni)," Phys. Rev. Mater. **2**, 075401 (2018).
[27]H.-K. Lyeo, D. G. Cahill, B.-S. Lee, J. R. Abelson, M.-H. Kwon, K.-B. Kim, S. G. Bishop, and B.-k. Cheong, "Thermal conductivity of phase-change material $Ge_2Sb_2Te_5$," Appl. Phys. Lett. **89**, 151904 (2006).
[28]S. Harish, K. Ishikawa, S. Chiashi, J. Shiomi, and S. Maruyama, "Anomalous thermal conduction characteristics of phase change composites with single-walled carbon nanotube inclusions," J. Phys. Chem. C **117**, 15409 (2013).
[29]R. Zhao, S. Kang, C. Wu, Z. Cheng, Z. Xie, Y. Liu, and D. Zhang, "Designable electrical/thermal coordinated dual-regulation based on liquid metal shape memory polymer foam for smart switch," Adv. Sci. **10**, 2205428 (2023).
[30]W. Luo, X. Zhang, T. Luo, B. Li, B. Wei, J. Zhang, and G. Zhu, "A flexible thermal interface material as the heat switch for solid-state cooling," Adv. Funct. Mater. **36**, e12421 (2025).
[31]P. Zhu, J. Zhang, B. Wei, B. Li, and G. Zhu, "Liquid metal enabled thermal switch for active thermal management," Int. J. Heat Mass Transfer **254**, 127654 (2026).
[32]W. Xiang, Y. Lu, H. Wang, X. Sun, S. Chen, Z. He, and J. Liu, "Liquid-metal-based magnetic fluids," Nat. Rev. Mater. **9**, 433 (2024).
[33]D. Kim, J. Jeong, S. K. Chung, and J. B. J. Lee, "Magnetic liquid metals: A review," Adv. Funct. Mater. **34**, 2311153 (2024).
[34]B. Ma, C. Xu, J. Chi, J. Chen, C. Zhao, and H. Liu, "A versatile approach for direct patterning of liquid metal using magnetic field," Adv. Funct. Mater. **29**, 1901370 (2019).
[35]Y. Zhang, S. Jiang, Y. Hu, T. Wu, Y. Zhang, H. Li, A. Li, Y. Zhang, H. Wu, Y. Ding *et al.*, "Reconfigurable magnetic liquid metal robot for high-performance droplet manipulation," Nano Lett. **22**, 2923 (2022).
[36]L. Hu, H. Wang, X. Wang, X. Liu, J. Guo, and J. Liu, "Magnetic liquid metals manipulated in the three-dimensional free space," ACS Appl. Mater. Interfaces **11**, 8685 (2019).